Local protein dynamics during microvesicle exocytosis in neuroendocrine cells

Agila Somasundaram and Justin W. Taraska*
Laboratory of Molecular Biophysics, National Heart, Lung, and Blood Institute, National Institutes of Health, Bethesda, MD 20892

ABSTRACT **Calcium-triggered exocytosis is key to many physiological processes, including neurotransmitter and hormone release by neurons and endocrine cells. Dozens of proteins regulate exocytosis, yet the temporal and spatial dynamics of these factors during vesicle fusion remain unclear. Here we use total internal reflection fluorescence microscopy to visualize local protein dynamics at single sites of exocytosis of small synaptic-like microvesicles in live cultured neuroendocrine PC12 cells. We employ two-color imaging to simultaneously observe membrane fusion (using vesicular acetylcholine ACh transporter tagged to pHluorin) and the dynamics of associated proteins at the moments surrounding exocytosis. Our experiments show that many proteins, including the SNAREs syntaxin1 and VAMP2, the SNARE modulator tomosyn, and Rab proteins, are preclustered at fusion sites and rapidly lost at fusion. The ATPase *N*-ethylmaleimide–sensitive factor is locally recruited at fusion. Interestingly, the endocytic Bin-Amphiphysin-Rvs domain–containing proteins amphiphysin1, syndapin2, and endophilins are dynamically recruited to fusion sites and slow the loss of vesicle membrane-bound cargo from fusion sites. A similar effect on vesicle membrane protein dynamics was seen with the overexpression of the GTPases dynamin1 and dynamin2. These results suggest that proteins involved in classical clathrin-mediated endocytosis can regulate exocytosis of synaptic-like microvesicles. Our findings provide insights into the dynamics, assembly, and mechanistic roles of many key factors of exocytosis and endocytosis at single sites of microvesicle fusion in live cells.**

Monitoring Editor
Thomas F. J. Martin
University of Wisconsin

Received: Dec 12, 2017
Revised: May 17, 2018
Accepted: May 29, 2018

INTRODUCTION

Exocytosis is the cellular process in which cytoplasmic membrane-bound vesicles fuse with the plasma membrane and release their contents into the extracellular space. During synaptic transmission, action potentials depolarize the presynaptic terminal triggering Ca^{2+} influx into the cell. Local elevations in intracellular Ca^{2+} cause synaptic vesicles (SVs) in the terminal to fuse with the plasma membrane, releasing neurotransmitters into the synaptic cleft (Jahn and Fasshauer, 2012). SV exocytosis is a carefully orchestrated process that involves multiple steps and dozens of proteins. SVs are small, ~50 nm in diameter, and contain a repertoire of proteins on their membranes (Takamori *et al.*, 2006). These vesicular membrane proteins and several cytoplasmic and plasma membrane-associated proteins play important roles in regulating SV exocytosis (Sudhof, 2013d).

Specifically, SNARE proteins are thought to drive SV fusion with the plasma membrane (Sudhof and Rothman, 2009). The vesicular SNARE, synaptobrevin (VAMP), and the plasma membrane SNAREs, syntaxin and synaptosomal–associated protein 25 (SNAP25), form a four-helical zippered complex that pulls the two lipid bilayers together resulting in fusion. The SNAREs are sufficient for fusion in vitro (van den Bogaart *et al.*, 2010). However, under physiological conditions, several proteins, such as Rabs and their effector molecules (Fukuda, 2008), complexin (Trimbuch and Rosenmund, 2016), the Ca^{2+} sensor synaptotagmin (Sudhof, 2013a), tomosyn (Ashery *et al.*, 2009; Bielopolski *et al.*, 2014), Ca^{2+}-dependent activator protein for secretion (CAPS) (Stevens and Rettig, 2009), Munc18, and

This article was published online ahead of print in MBoC in Press (http://www.molbiolcell.org/cgi/doi/10.1091/mbc.E17-12-0716) on June 6, 2018.

Author contributions: A.S. and J.W.T. designed the study, A.S. performed experiments, and A.S. and J.W.T. analyzed data and wrote the manuscript.

*Address correspondence to: Justin Taraska (justin.taraska@nih.gov).

Abbreviations used: CME, clathrin-mediated endocytosis; LDCV, large dense core vesicle; SLMV, synaptic-like microvesicle; SV, synaptic vesicle; TIRF, total internal reflection fluorescence; VAChT, vesicular acetylcholine transporter.

© 2018 Somasundaram and Taraska. This article is distributed by The American Society for Cell Biology under license from the author(s). Two months after publication it is available to the public under an Attribution–Noncommercial–Share Alike 3.0 Unported Creative Commons License (http://creativecommons.org/licenses/by-nc-sa/3.0).

"ASCB®," "The American Society for Cell Biology®," and "Molecular Biology of the Cell®" are registered trademarks of The American Society for Cell Biology.

Munc13 (Sudhof and Rothman, 2009), have been proposed to regulate the steps leading to fusion, including docking (attaching the SV to the active zone) and priming (preparing the SV for fusion) (Sudhof, 2013d). While much is known about the biochemical properties of these proteins and their physiological effects, a comprehensive understanding of their spatial and temporal dynamics during SV exocytosis in live cells is lacking, partly due to the small size of the SVs and the challenges associated with labeling and imaging single vesicles in synaptic terminals (Kavalali and Jorgensen, 2014). Understanding the dynamics of these key mediators of SV exocytosis will provide direct insights into their regulatory functions, biological mechanisms, and roles in disease.

Neuroendocrine PC12 cells have two distinct Ca^{2+}-triggered exocytic vesicle pools, ~50-nm-diameter synaptic-like microvesicles (SLMVs) and the larger ~150-nm-diameter dense core vesicles (DCVs) (Thomas-Reetz and De Camilli, 1994). Both vesicle populations fuse with the plasma membrane with a rise in intracellular Ca^{2+}. However, each vesicle-type exhibits distinct Ca^{2+} sensitivities and fusion kinetics and is responsible for the release of different signals (Ninomiya *et al.*, 1997). Specifically, DCVs release peptide neurotransmitters, proteins, and amines while microvesicles release the chemical neurotransmitter acetylcholine (ACh) or γ-aminobutyric acid. Furthermore, SLMVs are stimulated at much lower intracellular Ca^{2+} concentrations, allowing for a more rapid burst of fusion during depolarization (Ninomiya *et al.*, 1997). SLMVs are structurally and functionally similar to neuronal SVs (Thomas-Reetz and De Camilli, 1994). They maintain an acidic pH, accumulate neurotransmitters, and fuse with the plasma membrane to release their luminal contents in a Ca^{2+}-dependent manner. Furthermore, they contain many of the same proteins required for cargo packaging, transport, exocytosis, and recycling, but unlike SVs, SLMVs do not appear clustered at active zones via synapsins (Thomas-Reetz and De Camilli, 1994). Aside from the interest in their signaling functions in endocrine cells, these vesicles have been used as experimentally tractable surrogates for the study of SV behavior (de Wit *et al.*, 2001; Brauchi *et al.*, 2008; Sochacki *et al.*, 2012). Here we used total internal reflection fluorescence (TIRF) microscopy to monitor the dynamics of over two dozen proteins during Ca^{2+}-triggered exocytosis of single SLMVs in PC12 cells (Sochacki *et al.*, 2012; Trexler *et al.*, 2016). In an imaging-based screen examining key exocytic and endocytic proteins, we show that many proteins, including syntaxin, VAMP, tomosyn, and Rab GTPases, are preclustered at fusion sites and rapidly diffuse away following exocytosis. Interestingly, Bin-Amphiphysin-Rvs (BAR) domain–containing proteins, and dynamin, known to be important in clathrin-mediated endocytosis, are recruited during fusion and influence the loss of vesicle membrane proteins from the fusion sites. Our study provides insights into the local dynamics, assembly, and function of key regulators of exocytosis and endocytosis during microvesicle fusion in live cells.

RESULTS

To image microvesicle fusion in PC12 cells, we expressed the vesicular ACh transporter (VAChT) tagged on its luminal side to pHluorin, a pH-sensitive variant of green fluorescent protein (GFP) (Miesenbock *et al.*, 1998). VAChT is targeted specifically to SLMVs in PC12 cells (Liu and Edwards, 1997), and VAChT-pHluorin has been used to track SLMV exocytosis (Brauchi *et al.*, 2008; Sochacki *et al.*, 2012). pHluorin fluorescence is quenched in the acidic lumen of the vesicle, but on fusion the lumenal pH is neutralized by the extracellular buffer causing pHluorin signal to dramatically increase, enabling the detection of exocytic events. To stimulate exocytosis, we depolarized cells by applying buffer containing high extracellular KCl using a superfusion pipette positioned close to the cell (Trexler *et al.*, 2016; Trexler and Taraska, 2017). Membrane depolarization caused a substantial increase in the frequency of fusion events as shown in Supplemental Figure 1A. Fusion events were detected as sudden bright flashes of green fluorescence (Figure 1A). This is observed as a local sharp increase in signal that decays with time as VAChT-pH diffuses away from the sites of exocytosis (Figure 1A, bottom, and Supplemental Figure 1B). In the red fluorescent channel, we monitored coexpressed proteins fused to mCherry, mRFP, or mKate2 (Supplemental Figure 1D table). In the example shown in Figure 1, VAChT-pH was coexpressed with mRFP-Rab3A (Figure 1B), where measurable changes in signal were detected during fusion (Figure 1B, bottom). Background-subtracted fluorescence intensities from hundreds of individual fusion events were extracted, normalized, and averaged in the green and red channels for every protein examined in the study to produce the average time-dependent changes in local protein signals at fusion sites (Figure 1, C and D). We analyzed ~8000 fusion events from over 300 cells to track, quantitate, and characterize the dynamics of dozens of proteins (Supplemental Figure 1D table). To verify that fusion events predominantly occurred from microvesicles in our experimental system, we stimulated PC12 cells coexpressing VAChT-pHuji and neuropeptide Y (NPY) tagged to GFP (to label large dense core vesicles [LDCVs]) (Shen *et al.*, 2014; Martineau *et al.*, 2017). As expected, VAChT-labeled fusion events were detected in the pHuji channel (23 events in four cells), but not in the NPY-GFP channel, and no specific increase in GFP signal was measured in regions corresponding to VAChT-labeled events (Supplemental Figure 1C). These results further confirm that VAChT is a specific marker of exocytic SLMVs in PC12 cells.

Rab GTPases and effectors are rapidly lost from sites of SLMV exocytosis

We first examined the dynamics of the Rab family of GTPases and Rab effector molecules, which play important roles in targeting and docking synaptic vesicles to the plasma membrane (Fukuda, 2008). In PC12 cells, Rab27A and Rab3A were localized at exocytic sites before fusion and diffused away rapidly following exocytosis, consistent with their vesicle membrane-anchored nature (Figure 2, A and B, and Supplemental Figure 2). The cytosolic Rab3A effector molecule, Rabphilin3A, also displayed similar localization and behavior (Figure 2C and Supplemental Figure 2). An early endosomal Rab, Rab5A (Woodman, 2000), showed some enrichment at fusion sites that slowly decreased following fusion (Figure 2D, Supplemental Figure 2). Rab27B did not exhibit specific localization at SLMVs or a change in intensity following fusion (Figure 2E and Supplemental Figure 2). These results demonstrate that the Rab proteins, Rab27A and Rab3A, and the effector Rabphilin3A, are targeted to microvesicle sites before exocytosis and are dynamically lost into the cytosol or plasma membrane following fusion.

SNAREs, syntaxin1 and VAMP2, are clustered at fusion sites and lost following fusion

Docked vesicles fuse with the plasma membrane by the concerted action of the SNARE proteins syntaxin, SNAP25, and VAMP2 (Sudhof and Rothman, 2009). We found that the plasma membrane SNARE, syntaxin1, decreased in intensity at fusion sites during exocytosis (Figure 3A). Similar to the distribution seen in LDCVs (Lang *et al.*, 2001; Barg *et al.*, 2010; Gandasi and Barg, 2014; Ullrich *et al.*, 2015), radial scan analysis of syntaxin1 fluorescence revealed locally elevated syntaxin1 that diffused away following fusion, indicating that syntaxin1 is clustered on the plasma membrane at sites of microvesicle exocytosis (Supplemental Figure 3). We did not observe reclustering of syntaxin1 at the original fusion sites (Supplemental Figure 3).

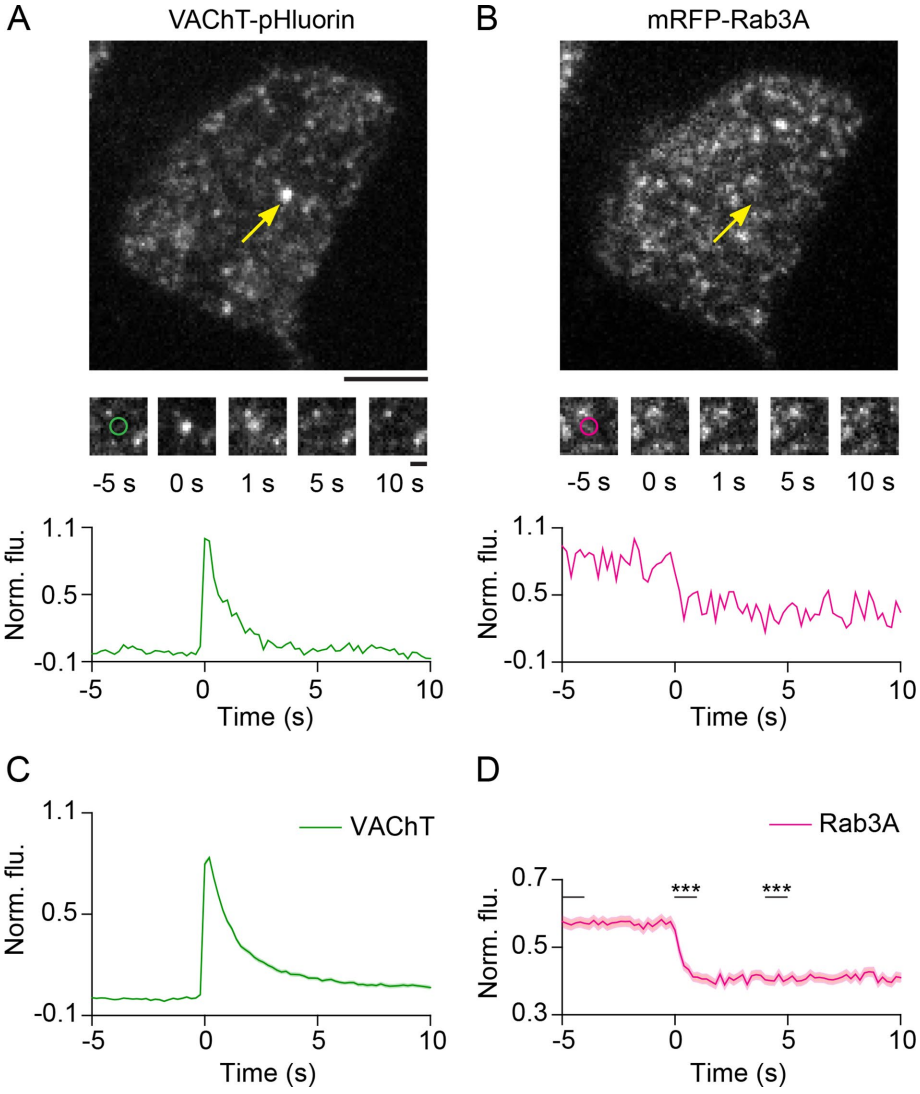

FIGURE 1: Analysis of protein dynamics at SLMV fusion sites in PC12 cells. (A, B) Images of a PC12 cell transfected with VAChT-pH (A) and mRFP-Rab3A (B) imaged using TIRF microscopy. Arrows (yellow) show a fusion event in the green channel and the corresponding region in the red channel, after application of stimulation buffer. Bar, 5 µm. Middle, snapshots of the fusion event shown above at the indicated time points. Time-point "0 s" indicates the manually identified first frame of brightening in the green channel. Circles (~1 µm diameter) represent regions used for intensity analysis. Bar, 1 µm. Bottom, time-lapse traces of normalized fluorescence intensities for the event shown above in the green and red channels.
(C, D) Average time-lapse traces of normalized fluorescence intensities for VAChT-pH (green) and mRFP-Rab3A (magenta) (196 events, five cells). Individual event traces were time aligned to 0 s, which corresponds to the fusion frame in the green channel. Standard errors are plotted as shaded areas around the average traces. ***$p \leq 0.0001$ when compared with baseline.

The plasma membrane-attached SNARE, SNAP25, did not exhibit increased localization at fusion sites or a substantial change in signal or distribution during fusion (Figure 3B and Supplemental Figure 3). VAMP2 showed some concentration at fusion sites, consistent with its expression on the vesicular membrane, and diffused away following fusion (Figure 3C and Supplemental Figure 3). To rule out potential artifacts induced by the red fluorescent tag, we examined the distribution and dynamics of cytosolic mCherry and membrane-attached farnesyl-mCherry during fusion. Cytosolic mCherry was diffusely distributed both before and during fusion and showed a small increase in signal following fusion (Figure 3D and Supplemental Figure 3) likely due to mCherry diffusing into cytoplasmic space previously occupied by microvesicles (Taraska *et al.*, 2003). Farnesyl-mCherry signal increased slightly during fusion, perhaps due to the delivery of a small amount of probe contained on the vesicle to the plasma membrane (Figure 3E and Supplemental Figure 3). Thus, the control mCherry proteins exhibited small changes in signal during fusion that are markedly different from the dynamics of syntaxin1 and VAMP2 described above. In conclusion, the SNAREs syntaxin1 and VAMP2 are locally preassembled at microvesicle fusion sites and diffuse away from the sites of release.

SNARE modulators exhibit diverse behaviors during SLMV fusion

SNARE-mediated fusion is regulated by several proteins (Sudhof, 2013d). To gain insights into the function of these SNARE modulators in live cells, we next examined their dynamics during SLMV fusion in PC12 cells. Multiple roles have been proposed for the small protein complexin, which is thought to either clamp the SNARE complex in a partially zippered state, or facilitate fusion (Brose, 2008; Yoon *et al.*, 2008; An *et al.*, 2010; Wragg *et al.*, 2013). Complexin2 signal decreases slightly during fusion (Figure 4A); however, most of the protein appeared diffusely distributed before and after fusion (Supplemental Figure 5). A small decrease in signal was also seen with CAPS (Figure 4B), a protein essential for SV priming (Jockusch *et al.*, 2007). Unlike complexin2, CAPS displayed some preferential localization at fusion sites at rest (Supplemental Figure 5). The Ca^{2+} sensor synaptotagmin1 (Sudhof, 2013a) was concentrated at fusion sites but, surprisingly, did not diffuse away following fusion (Supplemental Figures 4A and 5). Tomosyn, thought to play a largely inhibitory role in SV priming (Gracheva *et al.*, 2006; McEwen *et al.*, 2006; Ashery *et al.*, 2009; Bielopolski *et al.*, 2014; Cazares *et al.*, 2016), was located as clusters at vesicles and diffused away following fusion (Figure 4C and Supplemental Figure 5). Munc18a and Munc13, proteins proposed to bind the SNAREs and have essential roles in SV fusion (Sudhof and Rothman, 2009), did not exhibit significant changes in dynamics during fusion (Supplemental Figures 4, B and C, and 5). Interestingly, the ATPase *N*-ethylmaleimide–sensitive factor (NSF) was transiently recruited to fusion sites during exocytosis (Figure 4D and Supplemental Figure 5), consistent with its role in disassembling SNARE complexes (Ryu *et al.*, 2016). Overall, SNARE modulators exhibited diverse and subtle behaviors, with some preassembled at fusion sites and lost following fusion (CAPS and tomosyn), some recruited to fusion sites (NSF), and others localized at fusion sites throughout fusion (synaptotagmin1). These data likely reflect the diverse functions of these distinct classes of proteins along with the transient and stepwise nature of their activities during microvesicle fusion.

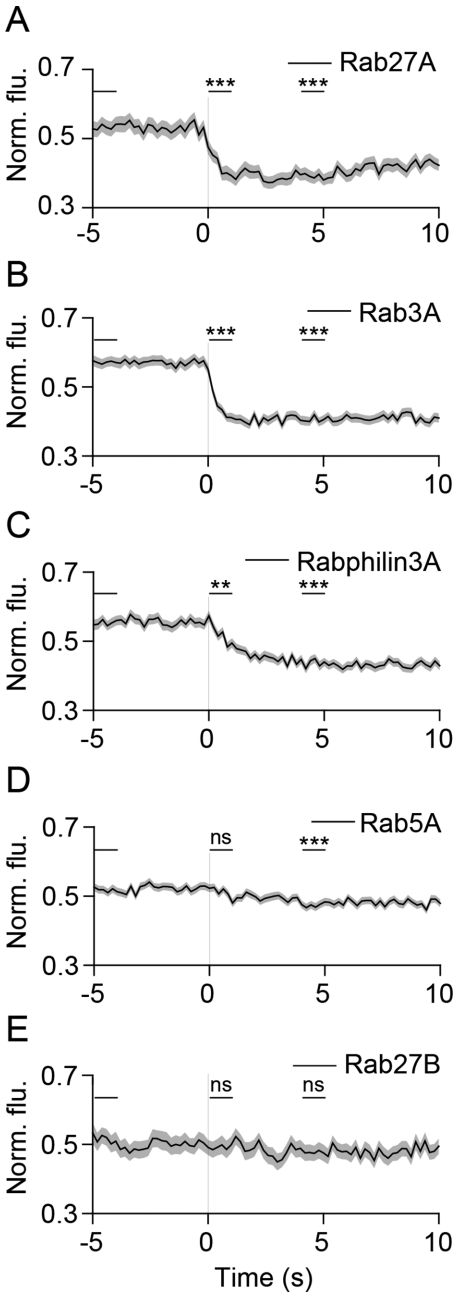

FIGURE 2: Dynamics of Rab proteins during SLMV fusion. (A–E) Average time-lapse traces of normalized fluorescence intensities for (A) mCherry-Rab27A (103 events, four cells), (B) mRFP-Rab3A (196 events, five cells), (C) mCherry-Rabphilin3A (198 events, six cells), (D) mCherry-Rab27B (73 events, three cells), and (E) mCherry-Rab5A (276 events, six cells). Individual event traces were time aligned to 0 s (vertical black line), which corresponds to the fusion frame in the green channel. Standard errors are plotted as shaded areas around the average traces. $^{**}p \leq 0.01$, $^{***}p \leq 0.0001$, ns, not significant, when compared with baseline.

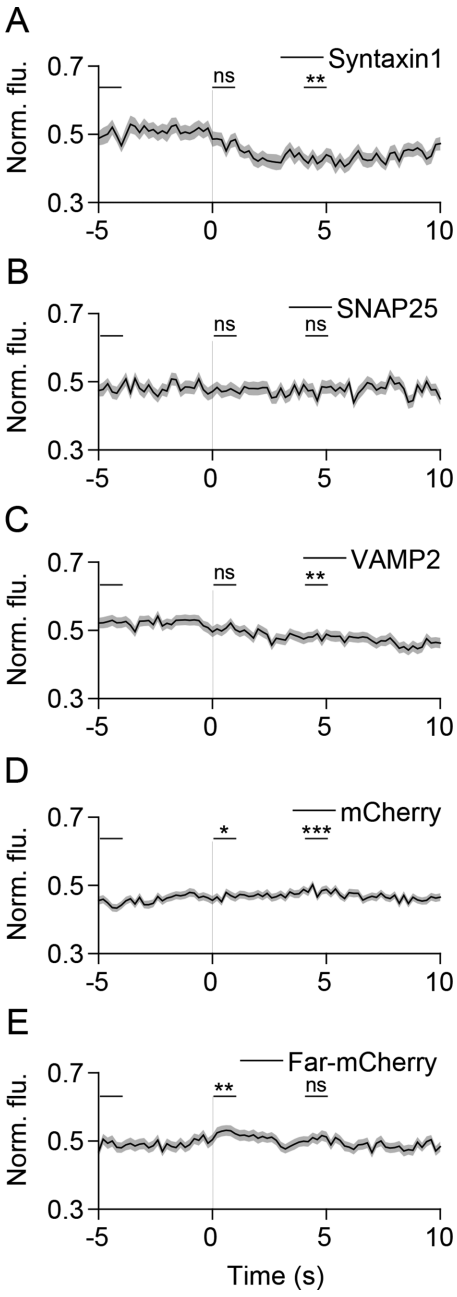

FIGURE 3: SNAREs syntaxin1 and VAMP2 diffuse away from sites of SLMV fusion. (A–E) Average time-lapse traces of normalized fluorescence intensities for (A) dCMV-mCherry-syntaxin1 (76 events, four cells), (B) dCMV-mCherry-SNAP25 (97 events, eight cells), (C) VAMP2-mCherry (172 events, 7 cells), (D) mCherry (274 events, eight cells), and (E) farnesyl-mCherry (166 events, nine cells). Individual event traces were time-aligned to 0 s (vertical black line), which corresponds to the fusion frame in the green channel. Standard errors are plotted as shaded areas around the average traces. $^{*}p \leq 0.05$, $^{**}p \leq 0.01$, $^{***}p \leq 0.0001$, ns, not significant, when compared with baseline.

BAR domain proteins are recruited to sites of SLMV exocytosis

Previous studies have shown that the proteins amphiphysin, syndapin, and dynamin, involved in the maturation and scission of clathrin-coated endocytic structures (McMahon and Boucrot, 2011; Daumke *et al.*, 2014), are recruited to exocytic sites (Tsuboi *et al.*, 2004; Jaiswal *et al.*, 2009; Trexler *et al.*, 2016) and regulate Ca^{2+}-dependent cargo release from LDCVs in endocrine cells (Graham *et al.*, 2002; Holroyd *et al.*, 2002; Tsuboi *et al.*, 2004; Min *et al.*, 2007; Fulop *et al.*, 2008; Llobet *et al.*, 2008; Anantharam *et al.*, 2010, 2011; Samasilp *et al.*, 2012; Trexler *et al.*, 2016) and constitutive secretion from post-Golgi vesicles (Jaiswal *et al.*, 2009). Because SLMVs are approximately fivefold smaller than LDCVs and likely have different

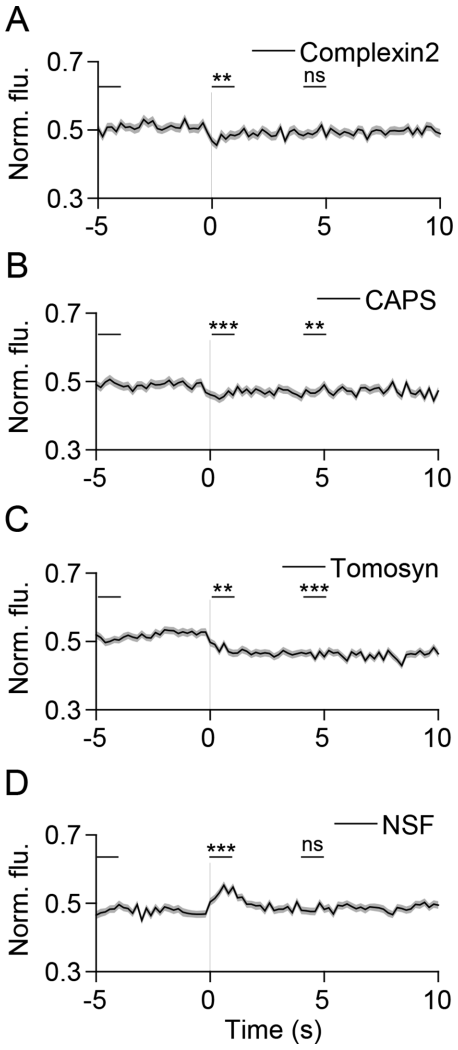

FIGURE 4: SNARE modulators exhibit diverse behaviors during SLMV fusion. (A–C) Average time-lapse traces of normalized fluorescence intensities for (A) complexin2-mCherry (202 events, seven cells), (B) CAPS-mKate2 (232 events, five cells), (C) mCherry-tomosyn (289 events, nine cells), and (D) NSF-mCherry (274 events, five cells). Individual event traces were time aligned to 0 s (vertical black line), which corresponds to the fusion frame in the green channel. Standard errors are plotted as shaded areas around the average traces. $^{**}p \leq 0.01$, $^{***}p \leq 0.0001$, ns, not significant, when compared with baseline.

curvatures, we hypothesized that a distinct set of proteins might be recruited (Xu and Xu, 2008; Zhang and Jackson, 2010). We first imaged the dynamics of the curvature sensing/inducing BAR domain proteins amphiphysin1 and syndapin2. Both proteins were specifically recruited to microvesicles during exocytosis (Figure 5 and Supplemental Figure 6A). BAR domain proteins endophilinA1 and endophilinA2 were also recruited during fusion (Supplemental Figure 7, A and B). EndophilinB1, however, appeared localized at fusion sites even at rest and did not exhibit significant changes in dynamics during fusion (Supplemental Figure 7D). Overall, these results indicate that specific BAR domain proteins are recruited to SLMVs at exocytosis in neuroendocrine cells.

To determine whether amphiphysin1 and syndapin2 recruitment to the site of fusion is driven by the curvature-sensitive BAR domains (Daumke *et al.*, 2014), we imaged mutants lacking BAR domains. Unlike the wild-type (WT) proteins, Amph1-ΔBAR and Synd2-ΔBAR did not show specific localization at fusion sites during exocytosis (Figure 6, A–D, and Supplemental Figure 6A), indicating that the BAR domain is required for amphiphysin1 and syndapin2 recruitment. Deletion of the protein–protein interaction domain (SH3) (David *et al.*, 1996; Grabs *et al.*, 1997; Qualmann *et al.*, 1999) in amphiphysin1 (Amph1-ΔSH3) and syndapin2 (Synd2-ΔSH3) did not prevent recruitment (Figure 6, E and F, and Supplemental Figure 6A), indicating that the SH3 domain is not required for their localization to SLMVs during fusion. Moreover, the BAR domain of syndapin2 (Synd2-BAR) showed strong recruitment (Figure 6H and Supplemental Figure 6A), whereas overexpression of the SH3 domain alone of amphiphysin1 (Amph1-SH3) did not show recruitment to fusion sites (Figure 6G and Supplemental Figure 6A). Thus, amphiphysin1 and syndapin2 recruitment is dependent on BAR domains, suggesting that these proteins could be targeted to the highly curved neck of the expanding fusion pore. Interestingly, recruitment appeared to slightly precede fusion (Figure 6), suggesting a possible localization of these proteins to a transient hemifusion state (Zhao *et al.*, 2016). Also, the retention of these proteins at fusion sites seconds after fusion (Figure 6 and Supplemental Figure 6A) suggests either the persistence of a curved neck of the fusion pore or the rapid formation of endocytic structures at or near the fusion sites (Watanabe *et al.*, 2013a, c). Radial scan analysis shows diffusional spread of VAChT-pH following fusion in the presence of Synd2-BAR (Supplemental Figure 6B), suggesting that at least some vesicular proteins can leave the sites of microvesicle exocytosis.

BAR domain proteins modulate loss of SLMV membrane cargo from fusion sites

We next investigated whether the recruitment of BAR domain proteins described above impacts the loss of vesicle membrane cargo from fusion sites by measuring VAChT-pH fluorescence decay (Sochacki *et al.*, 2012). Expression of Amph1-WT did not significantly alter VAChT-pH loss when compared with farnesyl-mCherry (Supplemental Figures 8A and 10G, $\tau = 2.39 \pm 0.04$ s vs. $\tau = 2.33 \pm 0.04$ s). However, overexpression of Amph1-ΔBAR and Amph1-SH3, proteins that were not recruited to fusion sites (Figure 6 and Supplemental Figure 6), resulted in faster VAChT-pH decay when compared with WT (Figure 7A and Supplemental Figure 10G, $\tau = 1.36 \pm 0.06$ s, $\tau = 1.88 \pm 0.08$ s). On the other hand, overexpression of Amph1-ΔSH3, which was recruited to fusion sites (Figure 6 and Supplemental Figure 6), resulted in slower VAChT-pH decay (Figure 7A and Supplemental Figure 10G, $\tau = 3.12 \pm 0.05$ s). These results suggest that amphiphysin1 recruitment during SLMV fusion slows the loss of vesicle membrane proteins from fusion sites.

We obtained similar results with syndapin2. Like Amph1-WT, expression of Synd2-WT did not alter VAChT-pH decay when compared with farnesyl-mCherry (Supplemental Figures 8B and 10G, $\tau = 2.28 \pm 0.04$ s vs. $\tau = 2.33 \pm 0.04$ s). Synd2-ΔBAR, which was not recruited to fusion sites (Figure 6 and Supplemental Figure 6), exhibited VAChT decay slightly slower than Synd2-WT (Figure 7B and Supplemental Figure 10G, $\tau = 2.63 \pm 0.05$). However, Synd2-ΔSH3 and Synd2-BAR, which showed strong and specific recruitment to fusion sites (Figure 6 and Supplemental Figure 6), substantially slowed down VAChT decay (Figure 7B and Supplemental Figure 10G, $\tau = 3.43 \pm 0.07$ s, $\tau = 2.94 \pm 0.04$ s). Thus, the lack of the SH3 domain in amphiphysin1 and syndapin2 further slows down the loss of membrane cargo when compared with WT (Figure 7). Furthermore, the BAR domain proteins endophilinA1, endophilinA2 and endophilinB1 that showed recruitment or localization at fusion sites (Supplemental Figure 7), resulted

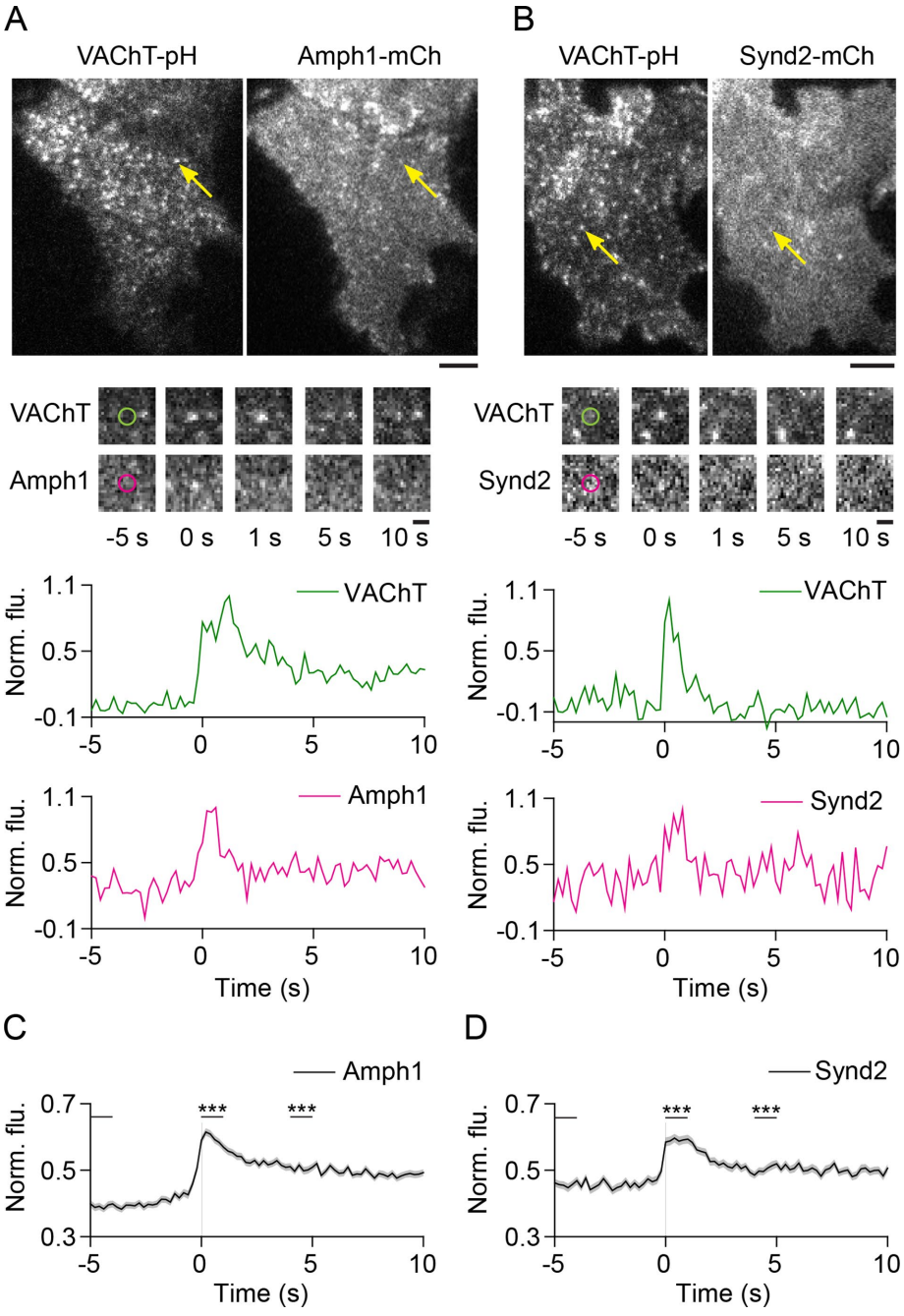

FIGURE 5: Amphiphysin1 and syndapin2 are transiently recruited to SLMV fusion sites. (A, B) Images of PC12 cells expressing (A) VAChT-pH and amphiphysin1-mCherry or (B) VAChT-pH and syndapin2-mCherry. Arrowheads show fusion events in the green channel and the corresponding regions in the red channel, after application of stimulation buffer. Bar, 5 μm. Middle, snapshots of the fusion event shown above at the indicated time points. Time-point "0 s" indicates the first frame of brightening in the green channel. Bar, 1 μm. Bottom, time-lapse traces of normalized fluorescence intensities in the green and red channels for the fusion event shown above. (C, D) Average time-lapse traces of normalized fluorescence intensities in the red channel for (C) Amph1-WT (371 events, nine cells) and (D) Synd2-WT (228 events, six cells). Individual event traces were time-aligned to 0 s (vertical black line), which corresponds to the fusion frame in the green channel. Standard errors are plotted as shaded areas around the average traces. ***$p \leq 0.0001$ when compared with baseline.

in significantly slower VAChT-pH decay when compared with farnesyl-mCherry (Supplemental Figures 8C and 10G, $\tau = 3.24 \pm 0.04$ s, $\tau = 3.07 \pm 0.06$ s, $\tau = 4.16 \pm 0.07$ s). Intriguingly, the VAChT-pH decay with farnesyl-mCherry was slower than with cytosolic mCherry (Supplemental Figures 8D and 10G, $\tau = 2.33 \pm 0.04$ s vs. 2.07 ± 0.10 s). It is possible that the small increase in farnesyl-mCherry seen during exocytosis (Figure 3 and Supplemental Figure 3) alters membrane properties including fluidity or packing to slow down cargo release (Stachowiak *et al.*, 2012). Because we are interested in the impact of membrane-associated BAR domain proteins on fusion dynamics, we chose to compare the resulting VAChT-pH decay profiles with that seen with farnesyl-mCherry (Supplemental Figure 8). Overall, our results indicate that BAR domain proteins slow the loss of vesicle membrane cargo from fusion sites during SLMV exocytosis.

We further examined the effects of knock-down of endogenous amphiphysin1 and syndapin2 on VAChT-pH loss by treating cells with small interfering RNA (siRNA) against these molecules. Western blot analysis revealed syndapin2 expression in PC12 cells, which was reduced with siRNA treatment (Supplemental Figure 9A). We were unsuccessful in our attempts to detect endogenous amphiphysin1 using commercial antibodies (unpublished data). Contrary to our expectation, the VAChT-pH decay in PC12 cells treated with siSyndapin2 was slower than that with control siRNA (Supplemental Figures 9B and 10G, $\tau = 4.01 \pm 0.06$ s vs. $\tau = 3.15 \pm 0.07$ s). It is possible that syndapin2 knock-down resulted in increased recruitment of other BAR domain proteins to fusion sites, but this complication was not explored further. Nonetheless, our experiments with amphiphysin1 and syndapin2 mutants, and endophilins, provide evidence for the modulation of microvesicle membrane cargo dynamics by BAR domain proteins.

Dynamin is recruited to fusion sites and delays loss of SLMV membrane cargo

Expression of amphiphysin1 and syndapin2 mutants lacking the SH3 domains resulted in slower VAChT-pH decay than that seen with full-length proteins (Figure 7), suggesting a role for SH3 binding partners in hastening the loss of VAChT from fusion sites. To test this hypothesis, we examined the dynamics of the well-studied SH3 binding partner, the GTPase dynamin (David *et al.*, 1996; Qualmann *et al.*, 1999; Ferguson and De Camilli, 2012). During clathrin-mediated endocytosis (CME), dynamin localizes to the curved neck of the invaginating clathrin-coated pit through its interactions with BAR domain proteins and causes scission (Daumke *et al.*, 2014). Dynamin1 and dynamin2 have also been shown to cluster at LDCV fusion sites (Holroyd *et al.*, 2002;

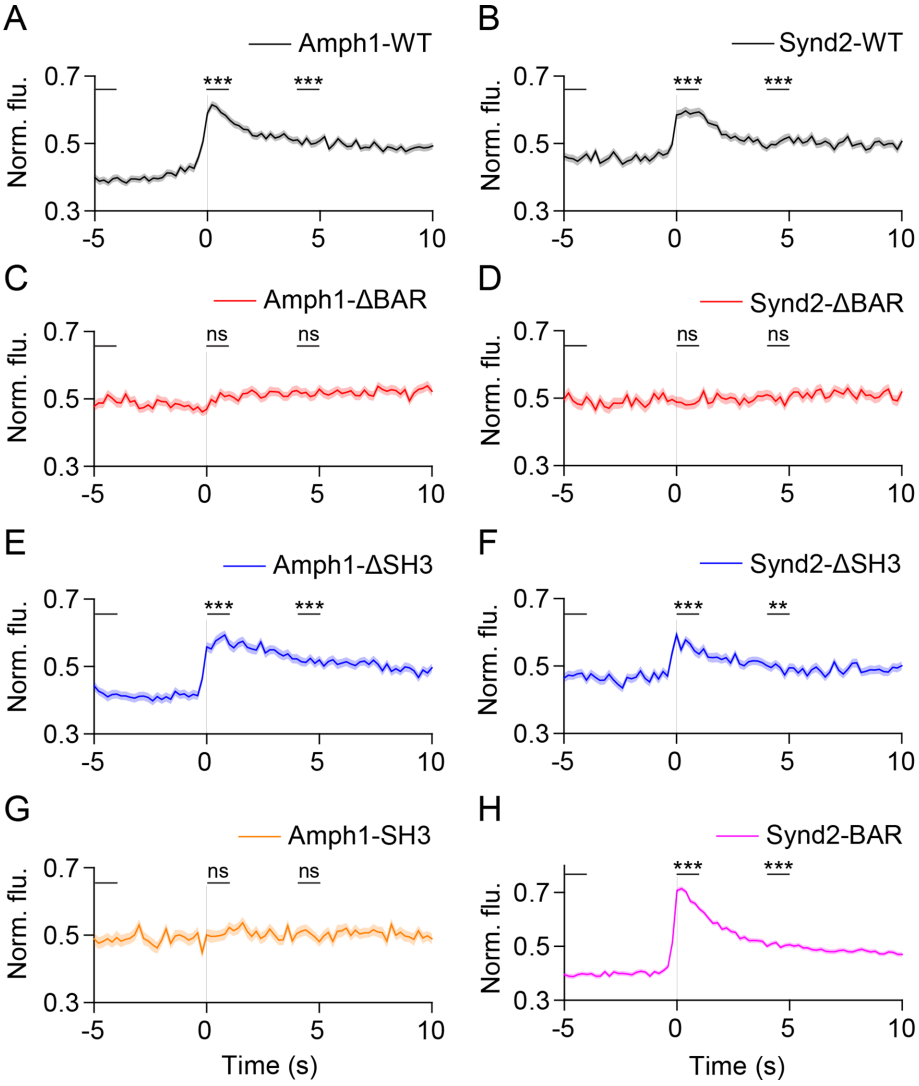

FIGURE 6: Amphiphysin1 and syndapin2 recruitment to SLMV fusion sites is dependent on the BAR domain. (A–H) Average time-lapse traces of normalized fluorescence intensities in the red channel for (A) Amph1-WT (371 events, nine cells), (B) Synd2-WT (228 events, six cells), (C) Amph1-ΔBAR (169 events, four cells), (D) Synd2-ΔBAR (136 events, 11 cells), (E) Amph1-ΔSH3 (214 events, 13 cells), (F) Synd2-ΔSH3 (184 events, nine cells), (G) Amph1-SH3 (117 events, eight cells), and (H) Synd2-BAR (418 events, 13 cells). Individual event traces were time-aligned to 0 s (vertical black line), which corresponds to the fusion frame in the green channel. Standard errors are plotted as shaded areas around the average traces. $^{**}p \leq 0.01$, $^{***}p \leq 0.0001$, ns, not significant, when compared with baseline.

Tsuboi *et al.*, 2004; Trexler *et al.*, 2016) and regulate fusion pore expansion (Holroyd *et al.*, 2002; Tsuboi *et al.*, 2004; Min *et al.*, 2007; Fulop *et al.*, 2008; Anantharam *et al.*, 2011; Samasilp *et al.*, 2012; Gonzalez-Jamett *et al.*, 2013; Fan *et al.*, 2015; Trexler *et al.*, 2016). We found that dynamin1 is transiently recruited to SLMVs during fusion (Supplemental Figure 10A) and slows down the loss of VAChT-pH when compared with control (Figure 8A and Supplemental Figure 10G, $\tau = 3.47 \pm 0.05$ s vs. $\tau = 2.33 \pm 0.04$ s). Dyn1-K44A, a GTPase mutant, was recruited to SLMV fusion sites (Supplemental Figure 10B), suggesting that the GTPase activity of dynamin1 is dispensable for its recruitment. Dyn1-K44A, however, hastened VAChT-pH decay (Figure 8B and Supplemental Figure 10G, $\tau = 2.09 \pm 0.08$ s). Thus, the recruitment of functional dynamin1 to SLMV fusion sites slows down loss of membrane cargo from the fusion site.

We next examined the effects of disrupting dynamin1's interactions with BAR domain proteins by mutating residues in its proline-rich domain (PRD) (Okamoto *et al.*, 1997). Dyn1 deficient in binding amphiphysin1 (Dyn1-833-838A, Dyn1-ΔAmph1) (Grabs *et al.*, 1997) showed mild localization at fusion sites, whereas dynamin1 deficient in binding syndapin2 (Dyn1-S774E/S778E, Dyn1-ΔSynd2) (Anggono *et al.*, 2006) exhibited substantial recruitment to SLMVs during fusion (Supplemental Figure 10, C and D). Both mutants, however, resulted in VAChT-pH decay that was comparable to that observed with Dyn1-WT (Figure 8B and Supplemental Figure 10G, $\tau = 3.68 \pm 0.05$ s, $\tau = 3.93 \pm 0.07$ s) and slower than with farnesyl-mCherry. Thus, our findings suggest that dynamin1 slows the loss of membrane cargo, and disrupting its interactions with either amphiphysin1 or syndapin2 does not lessen its effects.

Unlike dynamin1, dynamin2 (Dyn2-WT) did not show substantial recruitment to fusion sites (Supplemental Figure 10E). PC12 cells expressing Dyn2-WT, however, exhibited slower VAChT-pH decay when compared with farnesyl-mCherry (Figure 8C and Supplemental Figure 10G, $\tau = 3.56 \pm 0.09$ s vs. $\tau = 2.33 \pm 0.04$ s). This suggests that low levels of Dyn2-WT at fusion sites can affect cargo loss or that dynamin2 acts at a step prior to or distant from exocytosis. Dynamin2 lacking the PRD domain (Dyn2-ΔPRD) (Supplemental Figure 10F) resulted in faster loss of membrane cargo (Figure 8D and Supplemental Figure 10G, $\tau = 2.69 \pm 0.06$ s), suggesting that dynamin2's interaction with BAR domain proteins is essential for this effect. Taken together, these results suggest that dynamin1 and dynamin2 slow the loss of SLMV membrane cargo from fusion sites. This is consistent with the observation that Amph1-SH3, which sequesters SH3 binding partners such as dynamin (Shupliakov *et al.*, 1997; Wigge *et al.*, 1997; Holroyd *et al.*, 2002), results in faster VAChT-pH decay (Figure 7A). These results also suggest that the slower VAChT-pH decay seen in Amph1-ΔSH3 and Synd2-ΔSH3 mutants (Figure 7) lacking dynamin binding is likely due to a lack of interactions with SH3 binding partners other than dynamin.

Examination of the dynamics of neural Wiskott–Aldrich syndrome protein (N-WASP), a protein that binds SH3-domain containing proteins and stimulates actin polymerization during CME (Qualmann *et al.*, 1999; Kessels and Qualmann, 2002; Yamada *et al.*, 2009), did not reveal significant changes in signal or distribution during fusion (Supplemental Figure 11A) or a substantial change in the VAChT-pH decay when compared with control (Supplemental Figure 10G, $\tau = 2.64 \pm 0.05$ s, vs. $\tau = 2.33 \pm 0.04$ s). Interestingly, we observed a slow, but significant, increase in clathrin around fusion sites several seconds after fusion (Supplemental Figure 11B). Moreover, apart from the specific and transient recruitment of

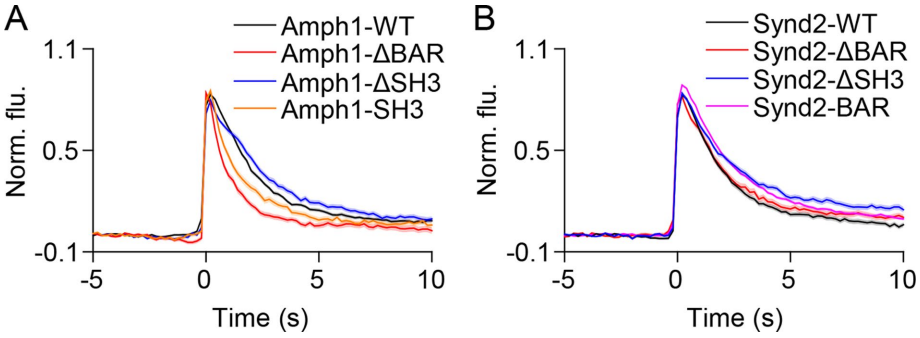

FIGURE 7: Amphiphysin1 and syndapin2 mutants slow the loss of VAChT-pH from fusion sites. (A) Average time-lapse traces of normalized VAChT-pH fluorescence intensities in PC12 cells coexpressing VAChT-pH and (A) WT or mutant amphiphysin1 and (B) WT or mutant syndapin2 constructs. Individual event traces were time aligned to 0 s, which corresponds to the frame of fusion. Standard errors are plotted as shaded areas around the average traces.

amphiphysin1 to fusion sites described earlier (Figure 5), in five of nine cells we observed a marked increase in amphiphysin1 clusters across the plasma membrane that peaked tens of seconds after stimulation and then disappeared (Supplemental Figure 12), suggesting compensatory endocytosis of released cargo or membrane, controlled by amphiphysin. This additional slow recruitment did not seem correlated to fusion sites. Last, the adaptor protein AP-2 and the scaffolding protein intersectin showed mild or no recruitment to fusion sites (Supplemental Figure 11, C and D), suggesting perhaps the presence of sufficient amounts of these proteins to effect endocytosis. Overall, our results support the model that BAR domain proteins and dynamin play important roles in modulating microvesicle membrane cargo dynamics in neuroendocrine cells.

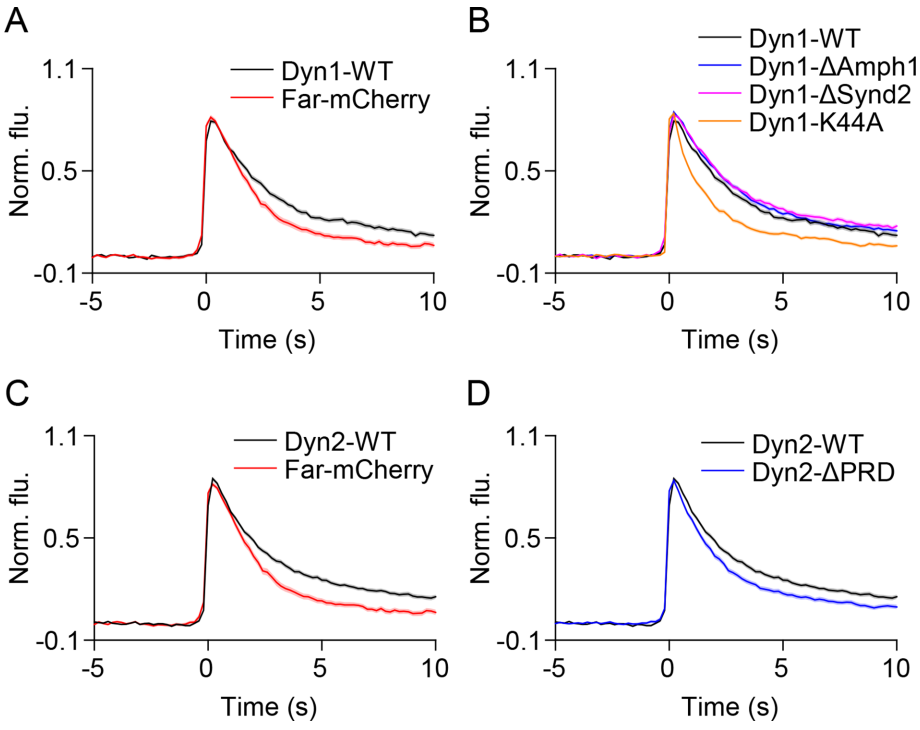

FIGURE 8: Dynamin1 and dynamin2 slow the loss of VAChT-pH from fusion sites. (A–D) Average time-lapse traces of normalized VAChT-pH fluorescence intensities in PC12 cells coexpressing VAChT-pH and (A, B) WT or mutant dynamin1 and (C, D) WT or mutant dynamin2 constructs. Individual event traces were time aligned to 0 s, which corresponds to the frame of fusion. Standard errors are plotted as shaded areas around the average traces.

DISCUSSION

Calcium-triggered exocytosis of SVs is a highly coordinated process involving dozens of proteins. The dynamics and assembly of these factors in live cells is not fully understood. Here we systematically analyzed the spatial and temporal dynamics of two dozen proteins around the moment of fusion of single SLMVs in living cells. Our experiments reveal distinct local dynamics of exocytic and endocytic proteins and a key role for BAR domain-containing proteins, along with dynamin, in modulating membrane cargo dynamics at microvesicle fusion sites.

First, we show that many proteins involved in SV exocytosis are concentrated at fusion sites several seconds before fusion (Lang *et al.*, 2001; Tsuboi and Rutter, 2003; Barg *et al.*, 2010; Gandasi and Barg, 2014; Ullrich *et al.*, 2015; Trexler *et al.*, 2016; Geerts *et al.*, 2017). These include the SNAREs, VAMP2 and syntaxin1 (Figure 3); the Ca sensor synaptotagmin1 (Supplemental Figure 4); the SNARE modulators tomosyn and CAPS (Figure 4); Rab proteins Rab3A and Rab27A; and the Rab effector molecule Rabphilin3A (Figure 2) (Supplemental Figures 2, 3, and 5). Because Rab proteins and VAMP2 are known to be associated with the vesicle membrane, their presence before fusion indicates that many SLMVs are docked at the plasma membrane prior to exocytosis. We did not measure additional recruitment of these molecules before fusion, suggesting that many proteins needed in exocytosis are preassembled at the vesicle. All these factors, except for synaptotagmin1, diffused away within seconds of fusion (Figures 2–4 and Supplemental Figures 2–5), indicating the highly dynamic and transient nature of the docking and fusion complex.

Synaptotagmin1 remained localized at fusion sites after fusion (Supplemental Figure 5), raising the possibility that SLMV fusion is incomplete. The complete release of VAChT-pH (Figure 1) suggests that classic kiss-and-run (Alabi and Tsien, 2013) is not the predominant mode of SLMV exocytosis in PC12 cells (Sochacki *et al.*, 2012). The residual VAChT-pH signal results from VAChT trapped in neighboring clathrin structures (Sochacki *et al.*, 2012). We cannot, however, rule out a cavicapture-type fusion mechanism (Holroyd *et al.*, 2002; Taraska *et al.*, 2003; Tsuboi *et al.*, 2004), where VAChT-pH is lost, but other components such as synaptotagmin1 are retained. Previous reports have suggested that synaptotagmin stays clustered after SV exocytosis (Willig *et al.*, 2006). Given that synaptotagmin1 is an important cargo for CME, it is possible that it is internalized very close to fusion sites through interactions with local adaptor proteins (Haucke and De Camilli, 1999; Martina *et al.*, 2001; McMahon and Boucrot, 2011). This is supported by the increase in clathrin at the plasma membrane seconds after fusion (Supplemental Figure 11).

We did not see clusters, or changes in the dynamics of SNAP25 at fusion sites (Figure 3 and Supplemental Figure 3). It is possible that high levels of endogenous SNAP25 prevent the concentration of overexpressed or labeled protein at fusion sites (Knowles *et al*., 2010). Surprisingly, we also did not see significant changes in signal for Munc18a and Munc13 (Supplemental Figures 4 and 5), molecules thought to be critical for vesicle docking and priming (Sudhof and Rothman, 2009; Gandasi and Barg, 2014), though Munc18a showed mild clustering at fusion sites (Supplemental Figure 5). This is different from the dynamics of these proteins observed with LDCVs in endocrine cells (Gandasi and Barg, 2014; Trexler *et al.*, 2016). It is possible that overexpression of these proteins masked small changes in signal. But a Munc18a construct with diminished promoter activity and reduced background signal also failed to show changes during fusion (unpublished data). The position and nature of the fluorescent tag could also interfere with its function (Crivat and Taraska, 2012). Detecting small transient dynamics of all proteins during fusion in this system will require future technical developments.

Of note, we found that the ATPase NSF is recruited at exocytosis (Figure 4 and Supplemental Figure 5). NSF and its binding partner α-soluble NSF-attachment protein (α-SNAP) (Sollner *et al*., 1993; Ungermann *et al*., 1998; Ryu *et al*., 2016) are thought to disassemble the SNARE complexes into monomeric SNAREs making them available for subsequent rounds of fusion (Ryu *et al*., 2016). It is unclear whether NSF acts after fusion (Littleton *et al*., 2001) or immediately prior to fusion (Banerjee *et al*., 1996; Kuner *et al*., 2008). Here the NSF signal appears to increase at fusion sites near the beginning of fusion (Figure 4 and Supplemental Figure 5) and stays elevated for ~2 s, suggesting that NSF activity is coupled to microvesicle exocytosis, both spatially and temporally.

Importantly, we show that curvature sensing BAR domain proteins and the GTPase dynamin are locally recruited to SLMV fusion sites. Specifically, we measure dynamic recruitment of amphiphysin1, syndapin2, endophilinA1, endophilinA2, and dynamin1 to SLMVs during fusion (Figures 5 and 6 and Supplemental Figures 6, 7, and 10). Amphiphysin1 and syndapin2 recruitment was dependent on their curvature sensing BAR domains (Figure 6 and Supplemental Figure 6), suggesting that these proteins are recruited to the curved membrane of the vesicle. EndophilinB1 appeared preclustered at fusion sites (Supplemental Figure 7), consistent with previous findings suggesting association of endophilins with SVs at rest in nerve terminals (Bai *et al*., 2010).

Furthermore, we show that the presence of BAR domain proteins and dynamin at fusion sites slows the loss of membrane cargo following exocytosis. Supporting this idea, overexpression of endophilinA1, endophilinA2, endophilinB1, dynamin1, and dynamin2 resulted in slower VAChT decay (Supplemental Figure 7 and Figure 8). Second, amphiphysin1 mutants that failed to assemble at fusion sites resulted in faster VAChT decay (Figure 7). Third, amphiphysin1 and syndapin2 mutants that lacked the SH3 domain but showed strong recruitment to fusion sites slowed down VAChT decay (Figure 7). Fourth, dynamin1 lacking its GTPase activity and, fifth, dynamin2 deficient in binding BAR domain proteins resulted in faster loss of VAChT at fusion sites (Figure 8). Amphiphysin1 and syndapin2 mutants lacking the SH3 domain (Figure 7) exhibited slower VAChT decay; however, the prominent SH3 binding proteins dynamin1 and dynamin2 resulted in even further delays (Figure 8), and N-WASP did not show significant recruitment (Supplemental Figure 11) or affect loss of VAChT from fusion sites, suggesting that interactions with other SH3 binding proteins (McPherson *et al*., 1994, 1996), lipids (Martin, 2015), or rearrangements in the cytoskeleton (Malacombe *et al*., 2006; Felmy, 2007; Wen *et al*., 2016; Gonzalez-Jamett *et al*., 2017) may be involved in modulating vesicle membrane cargo dynamics following fusion.

Because the loss of VAChT from fusion sites depends on both the rate of VAChT release from vesicles and the rate of VAChT diffusion in the plasma membrane, the delayed loss in the presence of BAR domain proteins and dynamins could be attributed to one or more of the following reasons. First, the recruitment of these proteins to the highly curved neck of the fusion pore could alter the structure of the pore and modulate cargo release. Such a model has been described previously for LDCVs (Wang *et al*., 2001; Llobet *et al*., 2008; Anantharam *et al*., 2010, 2011; Trexler *et al*., 2016). Specifically, in insulin-secreting beta cells, amphiphysin1, syndapin2, endophilinA2, dynamin1, and dynamin2 are recruited to LDCVs, and mutants of dynamin deficient in their interactions with BAR domain proteins hasten cargo release (Trexler *et al*., 2016). Moreover, in neurons, neurotransmitter release rates have been linked to the molecular machinery of the synaptic vesicle pore (Pawlu *et al*., 2004; Guzman *et al*., 2010). However, without a direct measure of microvesicle fusion pore properties in PC12 cells, it is unclear whether the recruitment of BAR domain proteins modulates membrane protein release and ACh release in a similar manner. Second, BAR domain proteins and dynamin could constrict the neck of the vesicle causing endocytosis in a cavicapture-type fusion model as described for LDCVs (Holroyd *et al*., 2002; Taraska *et al*., 2003; Taraska and Almers, 2004; Perrais *et al*., 2004; Tsuboi *et al*., 2004; Fulop *et al*., 2008) or alter the merger of the omega-profile with the plasma membrane (Chiang *et al*., 2014). Examination of radial scans reveals diffusion of VAChT away from fusion sites, even in the presence of the BAR domain (Supplemental Figure 6). It is possible that most of VAChT diffuses away, and the remaining vesicle components are endocytosed, or that there is heterogeneity in the vesicle population. The third possibility is that BAR domain proteins and dynamin are not recruited to the neck of the fusion pore but to sites very close to fusion but below the diffraction limit to effect endocytosis. This would be supported by the prolonged retention of BAR domain proteins at fusion sites (Supplemental Figure 6) and the delayed recruitment of clathrin (Supplemental Figure 11) and is consistent with previous studies demonstrating spatial and temporal proximity of exocytosis and compensatory endocytosis (Roos and Kelly, 1999; Sochacki *et al*., 2012; Watanabe *et al*., 2013a,c; Wu *et al*., 2014). And, last, BAR domain proteins and dynamin may have nonlocal effects on plasma membrane tension (Stachowiak *et al*., 2012), the cytoskeleton, or membrane fluidity, and affect fusion dynamics and/or diffusion of membrane cargo without directly modulating the fusion pore or endocytosis.

At the neuronal synapse, the association of endocytic proteins with SVs is thought to ensure the availability of these proteins for compensatory endocytosis (Shupliakov, 2009; Bai *et al*., 2010). Our findings that endocytic proteins are dynamically recruited to sites of fusing SLMVs, which are structurally and functionally similar to SVs (Thomas-Reetz and De Camilli, 1994), suggests that these proteins could play more active roles in modulating exocytosis, endocytosis, and the coupling between these two processes. Direct evaluation of the effects of endocytic protein recruitment on fusion pore dynamics and rapid compensatory endocytosis in neurons could provide insights into the complex regulation of synaptic membrane trafficking.

The protein dynamics observed at SLMV fusion sites is like that seen with the much larger LDCVs in endocrine cells. While SVs and LDCVs have broadly similar molecular requirements for fusion (Xu and Xu, 2008), differences in their size (~50 vs. ~150 nm

diameter), Ca^{2+} dependencies (Verhage *et al.*, 1991; Heidelberger *et al.*, 1994; Ninomiya *et al.*, 1997; Sudhof, 2013a), and latencies to fusion (Chow *et al.*, 1992; Sabatini and Regehr, 1996) suggest differential regulation of the exocytic fusion machinery. Furthermore, their different curvatures, pore sizes (19 vs. 213 pS conductance) (Klyachko and Jackson, 2002), and pore stabilities (Zhang and Jackson, 2010) suggest distinct structures of the pore. However, in both SLMVs and LDCVs, syntaxin1 (Lang *et al.*, 2001; Barg *et al.*, 2010; Gandasi and Barg, 2014), VAMP (Tsuboi and Rutter, 2003; Trexler *et al.*, 2016), Rab3A (Gandasi and Barg, 2014; Trexler *et al.*, 2016), Rab27A, Rabphilin3A, CAPS, and tomosyn (Trexler *et al.*, 2016) are concentrated at fusion sites and diffuse away following fusion, supporting parallels in the molecular assembly and disassembly of key components during LDCV and microvesicle exocytosis. Moreover, BAR domain proteins and dynamin are recruited to fusion sites of both SLMVs and LDCVs sites (Holroyd *et al.*, 2002; Tsuboi *et al.*, 2004; Trexler *et al.*, 2016). Given the different sensitivities to membrane curvature among the various BAR domain proteins (Daumke *et al.*, 2014) and dynamin isoforms (Yoshida *et al.*, 2004; Liu *et al.*, 2011), the differences in their assembly and effects on LDCV and SLMV exocytosis may be nuanced. For example, all three endophilins associated with fusing SLMVs, but only endophilinA2 localizes with LDCVs (Trexler *et al.*, 2016). Future work at higher temporal or spatial resolutions comparing LDCV and microvesicle fusion in the same cells, under expression-controlled conditions, will help identify key differences in protein dynamics needed to regulate different pools of vesicles, their fusion kinetics, release of their unique cargos, and their roles in signaling and cellular communication.

MATERIALS AND METHODS

Cells and solutions

PC12-GR5 cells were grown in DMEM containing 4 mM L-glutamine, supplemented with 5% fetal bovine serum (FBS), 5% horse serum, and 1% penicillin/streptomycin at 37°C in 5% CO_2. The cell line was originally obtained from Rae Nishi (Marine Biological Laboratory), expanded from low passage frozen stocks, and was not further authenticated. The cells tested negative for mycoplasma contamination. Cells were plated onto 25-mm, #1.5, round, poly-D-lysine–coated glass cover-slips and transfected ~24–48 h later with 1 µg each of the indicated plasmids, or 25 nmol of siRNA (Dharmacon), using Lipofectamine 2000 (Invitrogen) following the manufacturer's protocol. The list of plasmids used and the *n* values for all the experiments are listed in Supplemental Figure 1D. Cells were imaged ~24–48 h after transfection. The imaging buffer contained (in mM): 130 NaCl, 2.8 KCl, 5 $CaCl_2$, 1 $MgCl_2$, 10 HEPES, and 10 glucose. The pH was adjusted to 7.4 with 1 N NaOH. The stimulation buffer contained (in mM): 50 NaCl, 105 KCl, 5 $CaCl_2$, 1 $MgCl_2$, 10 HEPES, and 1 NaH_2PO_4. The pH was adjusted to 7.4 with 5 M KOH.

TIRF microscopy

TIRF microscopy was done as previously described (Trexler et al, 2016; Trexler and Taraska, 2017). Cells were imaged on an inverted fluorescent microscope (IX-81, Olympus), equipped with a ×100, 1.45 NA objective (Olympus). Combined green (488 nm) and red (561 nm) lasers (Melles Griot) were controlled with an acousto-optic tunable filter (Andor) and passed through a LF405/488/561/635 dichroic mirror. Emitted light was filtered using a 565 DCXR dichroic mirror on the image splitter (Photometrics), passed through 525Q/50 and 605Q/55 filters and projected onto the chip of an electron-multiplying charge-coupled device (EMCCD) camera. Images were acquired using the Andor IQ2 software. Cells were excited with alternate green and red excitation light, and images in each channel were acquired at 100-ms exposure at 5 Hz. To trigger exocytosis, stimulation buffer was applied for 30–40 s using a µFlow perfusion system (ALA Scientific Instruments) with a 100-µm pipette positioned close to the surface of the cell. Each day before experiments, 100-nm yellow-green fluorescent beads (Invitrogen) were imaged in the green and red channels and superimposed by mapping corresponding bead positions. The green and red cell images were aligned postacquisition using projective image transformation as described before (Sochacki et al, 2012; Trexler et al, 2016). All experiments were carried out at 25°C.

Image analysis

Image analysis was performed using Metamorph (Molecular Devices), ImageJ (National Institutes of Health), and custom scripts on MATLAB (Mathworks). The coordinates of the brightest pixel in the first frame of brightening for individual fusion events in the green channel were identified by eye and assigned as the center of the fusion event. All events were time aligned to the first frame of fusion (0 s). A circular region of interest (ROI) of 6 pixels (~990 nm) diameter and a square of 21 pixels (~3.5 µm) were drawn around the center, and the mean intensities in the surrounding square, excluding the circular region, were subtracted from the mean intensities in the center for each fusion event. This analysis was done for every frame from –10 to +50 s relative to the first frame of fusion. The background subtracted time-lapse intensities in the green channel were normalized 0–1 for each event, with "0" being the mean prefusion intensity, obtained from –5 to –3 s, and "1" being the peak intensity. The background subtracted time-lapse intensities for each event in the red channel were also normalized 0–1, with "0" being the minimum and "1" the maximum value, within –10 to +50 s. The resulting normalized traces were averaged across all events and truncated to show data from –5 to +10 s to better represent the protein dynamics around the moment of fusion. For the radial scan analyses, the intensities along 32 overlapping lines of 3.5 µm length arranged in a star pattern were averaged for each frame. The resulting kymograph through time for each event was normalized from 0–1000 and averaged across all events. Local background subtraction was not performed for radial scan analyses. The VAChT decay constants were obtained by single exponential fits of average VAChT fluorescence from 0.2 s to 5 s in the time-lapse traces, with y-offset constrained to 0, using OriginPro. Fusion events were excluded from time-lapse intensity analysis if one or more additional fusion events occurred in the circular ROI within 5 s before or after fusion (–5 to 5 s in the time-lapse traces). If additional events occurred >5 s after fusion, the original fusion event was not excluded from analysis. Therefore, the average intensities of VAChT and red proteins after 5 s in traces and radial scan images should be interpreted with this caveat in mind.

Western blots

PC12 cells were transfected with Syndapin2-GFP, or siRNA (Dharmacon) using Lipofectamine 2000, and protein was isolated ~24 h later. Cells were lysed in radioimmunoprecipitation assay (RIPA) buffer (1% Anatrace, 0.5% sodium deoxycholate, 0.1% SDS, 2 mM EDTA and 1 mM phenylmethylsulfonyl fluoride [PMSF] in PBS) on ice for 30 min. Lysates were centrifuged at 12,000 × *g* at 4°C for 10 min. Supernatants were boiled in lithium dodecyl sulfate (LDS) sample buffer containing 62.5 mM dithiothreitol (DTT) for 10 min and loaded onto 4–12% Tris-Bis gels (NuPAGE). Protein was transferred onto nitrocellulose membrane using the iBlot dry transfer system (ThermoFisher Scientific), and syndapin2 detected with monoclonal antibody (ThermoFisher Scientific) and peroxidase-labeled secondary

antibody. Blots were stripped with stripping buffer (ThermoFisher Scientific) and reprobed with α-actin antibody (Abcam).

Statistical tests

All data are expressed as mean ± SEM. Statistical analysis was done using two-tailed paired Student's *t* test to compare average normalized red protein fluorescence intensities at baseline (–5 to –4 s) with average intensities during (0 to 1 s), and after (4 to 5 s) fusion for the same set of events, as indicated in the figure legends.

ACKNOWLEDGMENTS

We thank Marie-Paule Strub (National Institutes of Health) for assistance with molecular biology; J. Silver, K. Sochacki, and A. Trexler for critical reading of the manuscript; and J. Silver, S. Kale, and members of the Taraska laboratory for discussions and input on data analysis methods. J.W.T. is supported by the Intramural Research Program of the National Heart, Lung, and Blood Institute, National Institutes of Health.

REFERENCES

Alabi AA, Tsien RW (2013). Perspectives on kiss-and-run: role in exocytosis, endocytosis, and neurotransmission. Annu Rev Physiol 75, 393–422.

An SJ, Grabner CP, Zenisek D (2010). Real-time visualization of complexin during single exocytic events. Nat Neurosci 13, 577–583.

Anantharam A, Bittner MA, Aikman RL, Stuenkel EL, Schmid SL, Axelrod D, Holz RW (2011). A new role for the dynamin GTPase in the regulation of fusion pore expansion. Mol Biol Cell 22, 1907–1918.

Anantharam A, Onoa B, Edwards RH, Holz RW, Axelrod D (2010). Localized topological changes of the plasma membrane upon exocytosis visualized by polarized TIRFM. J Cell Biol 188, 415–428.

Anggono V, Smillie KJ, Graham ME, Valova VA, Cousin MA, Robinson PJ (2006). Syndapin I is the phosphorylation-regulated dynamin I partner in synaptic vesicle endocytosis. Nat Neurosci 9, 752–760.

Ashery U, Bielopolski N, Barak B, Yizhar O (2009). Friends and foes in synaptic transmission: the role of tomosyn in vesicle priming. Trends Neurosci 32, 275–282.

Bai J, Hu Z, Dittman JS, Pym EC, Kaplan JM (2010). Endophilin functions as a membrane-bending molecule and is delivered to endocytic zones by exocytosis. Cell 143, 430–441.

Banerjee A, Barry VA, DasGupta BR, Martin TF (1996). N-Ethylmaleimide-sensitive factor acts at a prefusion ATP-dependent step in Ca2+-activated exocytosis. J Biol Chem 271, 20223–20226.

Barg S, Knowles MK, Chen X, Midorikawa M, Almers W (2010). Syntaxin clusters assemble reversibly at sites of secretory granules in live cells. Proc Natl Acad Sci USA 107, 20804–20809.

Bielopolski N, Lam AD, Bar-On D, Sauer M, Stuenkel EL, Ashery U (2014). Differential interaction of tomosyn with syntaxin and SNAP25 depends on domains in the WD40 beta-propeller core and determines its inhibitory activity. J Biol Chem 289, 17087–17099.

Brauchi S, Krapivinsky G, Krapivinsky L, Clapham DE (2008). TRPM7 facilitates cholinergic vesicle fusion with the plasma membrane. Proc Natl Acad Sci USA 105, 8304–8308.

Brose N (2008). For better or for worse: complexins regulate SNARE function and vesicle fusion. Traffic 9, 1403–1413.

Cazares VA, Njus MM, Manly A, Saldate JJ, Subramani A, Ben-Simon Y, Sutton MA, Ashery U, Stuenkel EL (2016). Dynamic partitioning of synaptic vesicle pools by the SNARE-binding protein Tomosyn. J Neurosci 36, 11208–11222.

Chiang HC, Shin W, Zhao WD, Hamid E, Sheng J, Baydyuk M, Wen PJ, Jin A, Momboisse F, Wu LG (2014). Post-fusion structural changes and their roles in exocytosis and endocytosis of dense-core vesicles. Nat Commun 5, 3356.

Chow RH, von Ruden L, Neher E (1992). Delay in vesicle fusion revealed by electrochemical monitoring of single secretory events in adrenal chromaffin cells. Nature 356, 60–63.

Crivat G, Taraska JW (2012). Imaging proteins inside cells with fluorescent tags. Trends Biotechnol 30, 8–16.

Daumke O, Roux A, Haucke V (2014). BAR domain scaffolds in dynamin-mediated membrane fission. Cell 156, 882–892.

David C, McPherson PS, Mundigl O, de Camilli P (1996). A role of amphiphysin in synaptic vesicle endocytosis suggested by its binding to dynamin in nerve terminals. Proc Natl Acad Sci USA 93, 331–335.

de Wit H, Lichtenstein Y, Kelly RB, Geuze HJ, Klumperman J, van der Sluijs P (2001). Rab4 regulates formation of synaptic-like microvesicles from early endosomes in PC12 cells. Mol Biol Cell 12, 3703–3715.

Fan F, Ji C, Wu Y, Ferguson SM, Tamarina N, Philipson LH, Lou X (2015). Dynamin 2 regulates biphasic insulin secretion and plasma glucose homeostasis. J Clin Invest 125, 4026–4041.

Felmy F (2007). Modulation of cargo release from dense core granules by size and actin network. Traffic 8, 983–997.

Ferguson SM, De Camilli P (2012). Dynamin, a membrane-remodelling GTPase. Nat Rev Mol Cell Biol 13, 75–88.

Fukuda M (2008). Regulation of secretory vesicle traffic by Rab small GTPases. Cell Mol Life Sci 65, 2801–2813.

Fulop T, Doreian B, Smith C (2008). Dynamin I plays dual roles in the activity-dependent shift in exocytic mode in mouse adrenal chromaffin cells. Arch Biochem Biophys 477, 146–154.

Gandasi NR, Barg S (2014). Contact-induced clustering of syntaxin and munc18 docks secretory granules at the exocytosis site. Nat Commun 5, 3914.

Geerts CJ, Mancini R, Chen N, Koopmans FTW, Li KW, Smit AB, van Weering JRT, Verhage M, Groffen AJA (2017). Tomosyn associates with secretory vesicles in neurons through its N- and C-terminal domains. PLoS One 12, e0180912.

Gonzalez-Jamett AM, Guerra MJ, Olivares MJ, Haro-Acuna V, Baez-Matus X, Vasquez-Navarrete J, Momboisse F, Martinez-Quiles N, Cardenas AM (2017). The F-actin binding protein cortactin regulates the dynamics of the exocytotic fusion pore through its SH3 domain. Front Cell Neurosci 11, 130.

Gonzalez-Jamett AM, Momboisse F, Guerra MJ, Ory S, Baez-Matus X, Barraza N, Calco V, Houy S, Couve E, Neely A, *et al.* (2013). Dynamin-2 regulates fusion pore expansion and quantal release through a mechanism that involves actin dynamics in neuroendocrine chromaffin cells. PLoS One 8, e70638.

Grabs D, Slepnev VI, Songyang Z, David C, Lynch M, Cantley LC, De Camilli P (1997). The SH3 domain of amphiphysin binds the proline-rich domain of dynamin at a single site that defines a new SH3 binding consensus sequence. J Biol Chem 272, 13419–13425.

Gracheva EO, Burdina AO, Holgado AM, Berthelot-Grosjean M, Ackley BD, Hadwiger G, Nonet ML, Weimer RM, Richmond JE (2006). Tomosyn inhibits synaptic vesicle priming in Caenorhabditis elegans. PLoS Biol 4, e261.

Graham ME, O'Callaghan DW, McMahon HT, Burgoyne RD (2002). Dynamin-dependent and dynamin-independent processes contribute to the regulation of single vesicle release kinetics and quantal size. Proc Natl Acad Sci USA 99, 7124–7129.

Guzman RE, Schwarz YN, Rettig J, Bruns D (2010). SNARE force synchronizes synaptic vesicle fusion and controls the kinetics of quantal synaptic transmission. J Neurosci 30, 10272–10281.

Haucke V, De Camilli P (1999). AP-2 recruitment to synaptotagmin stimulated by tyrosine-based endocytic motifs. Science 285, 1268–1271.

Heidelberger R, Heinemann C, Neher E, Matthews G (1994). Calcium dependence of the rate of exocytosis in a synaptic terminal. Nature 371, 513–515.

Holroyd P, Lang T, Wenzel D, De Camilli P, Jahn R (2002). Imaging direct, dynamin-dependent recapture of fusing secretory granules on plasma membrane lawns from PC12 cells. Proc Natl Acad Sci USA 99, 16806–16811.

Jahn R, Fasshauer D (2012). Molecular machines governing exocytosis of synaptic vesicles. Nature 490, 201–207.

Jaiswal JK, Rivera VM, Simon SM (2009). Exocytosis of post-Golgi vesicles is regulated by components of the endocytic machinery. Cell 137, 1308–1319.

Jockusch WJ, Speidel D, Sigler A, Sorensen JB, Varoqueaux F, Rhee JS, Brose N (2007). CAPS-1 and CAPS-2 are essential synaptic vesicle priming proteins. Cell 131, 796–808.

Kavalali ET, Jorgensen EM (2014). Visualizing presynaptic function. Nat Neurosci 17, 10–16.

Kessels MM, Qualmann B (2002). Syndapins integrate N-WASP in receptor-mediated endocytosis. EMBO J 21, 6083–6094.

Klyachko VA, Jackson MB (2002). Capacitance steps and fusion pores of small and large-dense-core vesicles in nerve terminals. Nature 418, 89–92.

Knowles MK, Barg S, Wan L, Midorikawa M, Chen X, Almers W (2010). Single secretory granules of live cells recruit syntaxin-1 and synaptosomal associated protein 25 (SNAP-25) in large copy numbers. Proc Natl Acad Sci USA 107, 20810–20815.

Kuner T, Li Y, Gee KR, Bonewald LF, Augustine GJ (2008). Photolysis of a caged peptide reveals rapid action of N-ethylmaleimide sensitive

factor before neurotransmitter release. Proc Natl Acad Sci USA 105, 347–352.
Lang T, Bruns D, Wenzel D, Riedel D, Holroyd P, Thiele C, Jahn R (2001). SNAREs are concentrated in cholesterol-dependent clusters that define docking and fusion sites for exocytosis. EMBO J 20, 2202–2213.
Littleton JT, Barnard RJ, Titus SA, Slind J, Chapman ER, Ganetzky B (2001). SNARE-complex disassembly by NSF follows synaptic-vesicle fusion. Proc Natl Acad Sci USA 98, 12233–12238.
Liu Y, Edwards RH (1997). Differential localization of vesicular acetylcholine and monoamine transporters in PC12 cells but not CHO cells. J Cell Biol 139, 907–916.
Liu YW, Neumann S, Ramachandran R, Ferguson SM, Pucadyil TJ, Schmid SL (2011). Differential curvature sensing and generating activities of dynamin isoforms provide opportunities for tissue-specific regulation. Proc Natl Acad Sci USA 108, E234–E242.
Llobet A, Wu M, Lagnado L (2008). The mouth of a dense-core vesicle opens and closes in a concerted action regulated by calcium and amphiphysin. J Cell Biol 182, 1017–1028.
Malacombe M, Bader MF, Gasman S (2006). Exocytosis in neuroendocrine cells: new tasks for actin. Biochim Biophys Acta 1763, 1175–1183.
Martin TF (2015). PI(4,5)P(2)-binding effector proteins for vesicle exocytosis. Biochim Biophys Acta 1851, 785–793.
Martina JA, Bonangelino CJ, Aguilar RC, Bonifacino JS (2001). Stonin 2: an adaptor-like protein that interacts with components of the endocytic machinery. J Cell Biol 153, 1111–1120.
Martineau M, Somasundaram A, Grimm JB, Gruber TD, Choquet D, Taraska JW, Lavis LD, Perrais D (2017). Semisynthetic fluorescent pH sensors for imaging exocytosis and endocytosis. Nat Commun 8, 1412.
McEwen JM, Madison JM, Dybbs M, Kaplan JM (2006). Antagonistic regulation of synaptic vesicle priming by Tomosyn and UNC-13. Neuron 51, 303–315.
McMahon HT, Boucrot E (2011). Molecular mechanism and physiological functions of clathrin-mediated endocytosis. Nat Rev Mol Cell Biol 12, 517–533.
McPherson PS, Czernik AJ, Chilcote TJ, Onofri F, Benfenati F, Greengard P, Schlessinger J, De Camilli P (1994). Interaction of Grb2 via its Src homology 3 domains with synaptic proteins including synapsin I. Proc Natl Acad Sci USA 91, 6486–6490.
McPherson PS, Garcia EP, Slepnev VI, David C, Zhang X, Grabs D, Sossin WS, Bauerfeind R, Nemoto Y, De Camilli P (1996). A presynaptic inositol-5-phosphatase. Nature 379, 353–357.
Miesenbock G, De Angelis DA, Rothman JE (1998). Visualizing secretion and synaptic transmission with pH-sensitive green fluorescent proteins. Nature 394, 192–195.
Min L, Leung YM, Tomas A, Watson RT, Gaisano HY, Halban PA, Pessin JE, Hou JC (2007). Dynamin is functionally coupled to insulin granule exocytosis. J Biol Chem 282, 33530–33536.
Ninomiya Y, Kishimoto T, Yamazawa T, Ikeda H, Miyashita Y, Kasai H (1997). Kinetic diversity in the fusion of exocytotic vesicles. EMBO J 16, 929–934.
Okamoto PM, Herskovits JS, Vallee RB (1997). Role of the basic, proline-rich region of dynamin in Src homology 3 domain binding and endocytosis. J Biol Chem 272, 11629–11635.
Pawlu C, DiAntonio A, Heckmann M (2004). Postfusional control of quantal current shape. Neuron 42, 607–618.
Perrais D, Kleppe IC, Taraska JW, Almers W (2004). Recapture after exocytosis causes differential retention of protein in granules of bovine chromaffin cells. J Physiol 560, 413–428.
Qualmann B, Roos J, DiGregorio PJ, Kelly RB (1999). Syndapin I, a synaptic dynamin-binding protein that associates with the neural Wiskott-Aldrich syndrome protein. Mol Biol Cell 10, 501–513.
Roos J, Kelly RB (1999). The endocytic machinery in nerve terminals surrounds sites of exocytosis. Curr Biol 9, 1411–1414.
Ryu JK, Jahn R, Yoon TY (2016). Review: Progresses in understanding N-ethylmaleimide sensitive factor (NSF) mediated disassembly of SNARE complexes. Biopolymers 105, 518–531.
Sabatini BL, Regehr WG (1996). Timing of neurotransmission at fast synapses in the mammalian brain. Nature 384, 170–172.
Samasilp P, Chan SA, Smith C (2012). Activity-dependent fusion pore expansion regulated by a calcineurin-dependent dynamin-syndapin pathway in mouse adrenal chromaffin cells. J Neurosci 32, 10438–10447.
Shen Y, Rosendale M, Campbell RE, Perrais D (2014). pHuji, a pH-sensitive red fluorescent protein for imaging of exo- and endocytosis. J Cell Biol 207, 419–432.
Shupliakov O (2009). The synaptic vesicle cluster: a source of endocytic proteins during neurotransmitter release. Neuroscience 158, 204–210.
Shupliakov O, Low P, Grabs D, Gad H, Chen H, David C, Takei K, De Camilli P, Brodin L (1997). Synaptic vesicle endocytosis impaired by disruption of dynamin-SH3 domain interactions. Science 276, 259–263.
Sochacki KA, Larson BT, Sengupta DC, Daniels MP, Shtengel G, Hess HF, Taraska JW (2012). Imaging the post-fusion release and capture of a vesicle membrane protein. Nat Commun 3, 1154.
Sollner T, Whiteheart SW, Brunner M, Erdjument-Bromage H, Geromanos S, Tempst P, Rothman JE (1993). SNAP receptors implicated in vesicle targeting and fusion. Nature 362, 318–324.
Stachowiak JC, Schmid EM, Ryan CJ, Ann HS, Sasaki DY, Sherman MB, Geissler PL, Fletcher DA, Hayden CC (2012). Membrane bending by protein-protein crowding. Nat Cell Biol 14, 944–949.
Stevens DR, Rettig J (2009). The Ca(2+)-dependent activator protein for secretion CAPS: do I dock or do I prime? Mol Neurobiol 39, 62–72.
Sudhof TC (2013a). A molecular machine for neurotransmitter release: synaptotagmin and beyond. Nat Med 19, 1227–1231.
Sudhof TC (2013d). Neurotransmitter release: the last millisecond in the life of a synaptic vesicle. Neuron 80, 675–690.
Sudhof TC, Rothman JE (2009). Membrane fusion: grappling with SNARE and SM proteins. Science 323, 474–477.
Takamori S, Holt M, Stenius K, Lemke EA, Gronborg M, Riedel D, Urlaub H, Schenck S, Brugger B, Ringler P, *et al.* (2006). Molecular anatomy of a trafficking organelle. Cell 127, 831–846.
Taraska JW, Almers W (2004). Bilayers merge even when exocytosis is transient. Proc Natl Acad Sci USA 101, 8780–8785.
Taraska JW, Perrais D, Ohara-Imaizumi M, Nagamatsu S, Almers W (2003). Secretory granules are recaptured largely intact after stimulated exocytosis in cultured endocrine cells. Proc Natl Acad Sci USA 100, 2070–2075.
Thomas-Reetz AC, De Camilli P (1994). A role for synaptic vesicles in non-neuronal cells: clues from pancreatic beta cells and from chromaffin cells. FASEB J 8, 209–216.
Trexler AJ, Sochacki KA, Taraska JW (2016). Imaging the recruitment and loss of proteins and lipids at single sites of calcium-triggered exocytosis. Mol Biol Cell 27, 2423–2434.
Trexler AJ, Taraska JW (2017). Two-color total internal reflection fluorescence microscopy of exocytosis in endocrine cells. Methods Mol Biol 1563, 151–165.
Trimbuch T, Rosenmund C (2016). Should I stop or should I go? The role of complexin in neurotransmitter release. Nat Rev Neurosci 17, 118–125.
Tsuboi T, McMahon HT, Rutter GA (2004). Mechanisms of dense core vesicle recapture following "kiss and run" ("cavicapture") exocytosis in insulin-secreting cells. J Biol Chem 279, 47115–47124.
Tsuboi T, Rutter GA (2003). Multiple forms of "kiss-and-run" exocytosis revealed by evanescent wave microscopy. Curr Biol 13, 563–567.
Ullrich A, Bohme MA, Schoneberg J, Depner H, Sigrist SJ, Noe F (2015). Dynamical organization of syntaxin-1A at the presynaptic active zone. PLoS Comput Biol 11, e1004407.
Ungermann C, Nichols BJ, Pelham HR, Wickner W (1998). A vacuolar v-t-SNARE complex, the predominant form in vivo and on isolated vacuoles, is disassembled and activated for docking and fusion. J Cell Biol 140, 61–69.
van den Bogaart G, Holt MG, Bunt G, Riedel D, Wouters FS, Jahn R (2010). One SNARE complex is sufficient for membrane fusion. Nat Struct Mol Biol 17, 358–364.
Verhage M, McMahon HT, Ghijsen WE, Boomsma F, Scholten G, Wiegant VM, Nicholls DG (1991). Differential release of amino acids, neuropeptides, and catecholamines from isolated nerve terminals. Neuron 6, 517–524.
Wang CT, Grishanin R, Earles CA, Chang PY, Martin TF, Chapman ER, Jackson MB (2001). Synaptotagmin modulation of fusion pore kinetics in regulated exocytosis of dense-core vesicles. Science 294, 1111–1115.
Watanabe S, Liu Q, Davis MW, Hollopeter G, Thomas N, Jorgensen NB, Jorgensen EM (2013a). Ultrafast endocytosis at Caenorhabditis elegans neuromuscular junctions. Elife 2, e00723.
Watanabe S, Rost BR, Camacho-Perez M, Davis MW, Sohl-Kielczynski B, Rosenmund C, Jorgensen EM (2013c). Ultrafast endocytosis at mouse hippocampal synapses. Nature 504, 242–247.
Wen PJ, Grenklo S, Arpino G, Tan X, Liao HS, Heureaux J, Peng SY, Chiang HC, Hamid E, Zhao WD, *et al.* (2016). Actin dynamics provides membrane tension to merge fusing vesicles into the plasma membrane. Nat Commun 7, 12604.
Wigge P, Vallis Y, McMahon HT (1997). Inhibition of receptor-mediated endocytosis by the amphiphysin SH3 domain. Curr Biol 7, 554–560.

Willig KI, Rizzoli SO, Westphal V, Jahn R, Hell SW (2006). STED microscopy reveals that synaptotagmin remains clustered after synaptic vesicle exocytosis. Nature 440, 935–939.
Woodman PG (2000). Biogenesis of the sorting endosome: the role of Rab5. Traffic 1, 695–701.
Wragg RT, Snead D, Dong Y, Ramlall TF, Menon I, Bai J, Eliezer D, Dittman JS (2013). Synaptic vesicles position complexin to block spontaneous fusion. Neuron 77, 323–334.
Wu LG, Hamid E, Shin W, Chiang HC (2014). Exocytosis and endocytosis: modes, functions, and coupling mechanisms. Annu Rev Physiol 76, 301–331.
Xu T, Xu P (2008). Searching for molecular players differentially involved in neurotransmitter and neuropeptide release. Neurochem Res 33, 1915–1919.
Yamada H, Padilla-Parra S, Park SJ, Itoh T, Chaineau M, Monaldi I, Cremona O, Benfenati F, De Camilli P, Coppey-Moisan M, *et al*. (2009). Dynamic interaction of amphiphysin with N-WASP regulates actin assembly. J Biol Chem 284, 34244–34256.
Yoon TY, Lu X, Diao J, Lee SM, Ha T, Shin YK (2008). Complexin and Ca2+ stimulate SNARE-mediated membrane fusion. Nat Struct Mol Biol 15, 707–713.
Yoshida Y, Kinuta M, Abe T, Liang S, Araki K, Cremona O, Di Paolo G, Moriyama Y, Yasuda T, De Camilli P, Takei K (2004). The stimulatory action of amphiphysin on dynamin function is dependent on lipid bilayer curvature. EMBO J 23, 3483–3491.
Zhang Z, Jackson MB (2010). Membrane bending energy and fusion pore kinetics in Ca(2+)-triggered exocytosis. Biophys J 98, 2524–2534.
Zhao WD, Hamid E, Shin W, Wen PJ, Krystofiak ES, Villarreal SA, Chiang HC, Kachar B, Wu LG (2016). Hemi-fused structure mediates and controls fusion and fission in live cells. Nature 534, 548–552.